RESEARCH PAPER

Mechanical properties of wire and arc additively manufactured high-strength steel structures

Johanna Müller[1] · Jonas Hensel[1] · Klaus Dilger[1]

Abstract

Additive manufacturing with steel opens up new possibilities for the construction sector. Especially direct energy deposition processes like DED-arc, also known as wire arc additive manufacturing (WAAM), is capable of manufacturing large structures with a high degree of geometric freedom, which makes the process suitable for the manufacturing of force flow-optimized steel nodes and spaceframes. By the use of high strength steel, the manufacturing times can be reduced since less material needs to be deposited. To keep the advantages of the high strength steel, the effect of thermal cycling during WAAM needs to be understood, since it influences the phase transformation, the resulting microstructure, and hence the mechanical properties of the material. In this study, the influences of energy input, interpass temperature, and cooling rate were investigated by welding thin walled samples. From each sample, microsections were analyzed, and tensile test and Charpy-V specimens were extracted and tested. The specimens with an interpass temperature of 200 °C, low energy input and applied active cooling showed a tensile strength of ∼ 860–900 MPa, a yield strength of 700–780 MPa, and an elongation at fracture between 17 and 22%. The results showed the formation of martensite for specimens with high interpass temperatures which led to low yield and high tensile strengths ($R_{p0.2}$ = 520–590 MPa, R_m = 780–940 MPa) for the specimens without active cooling. At low interpass temperatures, the increase of the energy input led to a decrease of the tensile and the yield strength while the elongation at fracture as well as the Charpy impact energy increased. The formation of upper bainite due to the higher energy input can be avoided by accelerated cooling while martensite caused by high interpass temperatures need to be counteracted by heat treatment.

Keywords WAAM · High strength steel · Thermal cycle · Mechanical properties · Interpass temperature · Energy input · Active cooling · DED-arc · Direct energy deposition

1 Introduction

Conventional manufacturing methods and the use of semi-finished products are currently state-of-the-art in the construction industry. With a view to future developments in architecture and construction, customized connections between different components made of different materials are required and gain importance. The new approaches of additive manufacturing in construction enable the free architectural design of steel components, such as thin shells [1] and complex force flow-optimized steel nodes [2–4]. For the manufacturing of those steel nodes, there is a variety of additive manufacturing technologies. They are called direct energy deposition (DED) processes and can generally be categorized via their energy source: DED-laser, DED-EB, and DED-arc. DED-arc processes use conventional welding processes like GMAW, GTAW, or GPAW and can be combined with a robotic handling system which gives them a high degree of geometric freedom and makes them suitable for the manufacturing of complex parts. Besides that, DED-arc processes, also called WAAM (wire arc additive manufacturing), have a high build up rate, and since they use conventional welding wire, there is a variety of available materials like different steels, aluminum, and titanium.

In the wire arc additive manufacturing of these geometries, the layer-by-layer build-up approach leads to repeated

heating of already deposited layers, which affects the mechanical properties of the parts to be manufactured [5–7]. Furthermore, the heat introduced cannot be dissipated by surrounding structures, as in the case of joint welds, but is primarily given off to the ambient air. Depending on the geometry or the ratio of surface to volume of the part to be produced, different temperature profiles are formed. Especially with regard to the construction industry, where the parts to be manufactured have huge dimensions, the manufacturing time is long hence the material is frequently exposed to higher temperatures for a long time. One possibility to shorten the manufacturing time is the use of high strength steel. Due to the high yield strength (≈ 790 MPa), the required material can be reduced so less material needs to be melted. Combined with an active cooling technology, the cooling rate from convection is increased, the heat does not stay in the structure for such a long time, which saves manufacturing time and may have a positive effect on the mechanical properties of the high strength steel.

## 2 Thermal influences during WAAM of steel structures

Steel transforms during cooling from high temperatures from cubic-face-centered γ-crystal austenite to cubic-room-centered ferrite and carbide with different morphologies. In the case of fast cooling rates, this results in generation of martensite or lower bainite, while slower cooling rates promote the formation of upper bainite, pearlite, or ferrite [8]. Depending on the chemical composition, especially for steels with a high content of C, Ni, N, or Mn, the temperature at which the martensitic transformation starts and ends is lowered. Austenite with dissolved carbon remains in the microstructure as a metastable phase. This retained, metastable austenite can transform to martensite either under load or at low temperatures. With regard to the layerwise build-up principle of WAAM and the long holding times at high temperatures in general, this mechanism is of particular interest, since the martensite finish temperature (M_f) is unlikely reached.

The cooling rate can either be measured in °C/s or, as it is typical for joint welding, the $t_{8/5}$-time is given. The $t_{8/5}$-time describes the time span during cooling from 800 to 500 °C. This temperature range is of particular interest as the time for cooling from the austenite area is one of the main influencing factors regarding the microstructure and thus the mechanical properties. In order to maintain the beneficial mechanical properties of fine-grained high strength steel, the formation of pearlite and ferrite needs to be avoided, thus long $t_{8/5}$-times, repeated heating, and long holding times at high temperatures are not favorable. During WAAM, frequent reheating of previously deposited layers occurs and the

microstructure is exposed to high temperatures for several times. Dai et al. [9] analyzed the phase transformations during the WAAM process using a HSLA steel. They sectioned the temperature zones of the investigated component during the building process in four different regions: the solidification zone, the complete austenization zone, a partial austentization zone, and a tempering zone. According to Dai et al., the fine-grained microstructure of the HSLA steel WAAM part resulted from rapid heating to the austenization zone. Ferrite transformed to austenite but, due to short holding times in the austenitization zone, this process could not be finished and un-austenitized ferrite nuclei remained leading to refined grains.

Studies on the properties of high strength steels as build-up material, such as ER120S-G/G 89 6 M21 Mn4Ni2CrMo ($R_{p0.2} > 890$ MPa) [10, 11], ER110S-G/G 69 4 M Mn3Ni1CrM ($R_{p0.2} > 710$ MPa) [12, 13], and ER100/G 69 6 M21 Mn4Ni1.5CrMo ($R_{p0.2} > 720$ MPa) [14], are available in the literature. It was investigated how the thermal cycles and the repeated heating of already deposited layers in 2-dimensional wall structures affect the microstructure and the mechanical properties. Yildiz et al. [10] investigated the influence of energy input on the microstructure, hardness, and tensile strength of ER120S-G. In this study, high energy input was used to determine its effect on the mechanical properties. They found a reduction in hardness resulting from high energy input compared to low energy input and a reduction of tensile and yield strength. The hardness tended to decrease with increasing distance to the base plate. According to Rodridues et al. [12], reheating can lead to recrystallization, resulting either in a fine-grained microstructure or, in the case of high peak temperatures, in coarse grain growth. Bourlet et al. [14] attribute the reduced yield strength of WAAM-HSLA steels to the presence of coarse-grained, allotropic ferrite and retained austenite. However, in this investigation, the interpass temperature was not kept constant. The structure was built up continuously, without waiting times between subsequent layers. This led to a heat accumulation and thus to temperatures exceeding 600 °C, which lasted longer than 30 min. In other investigations [10, 12, 13], the WAAM structure was not manufactured continuously, but with constant waiting times between the individual layers, causing the interpass temperature to rise as the structure was built. In [13], Duarte et al. proved the presence of retained austenite in samples produced with high energy input. The austenite volume fraction decreased with increasing distance to the base plate which could be referred to lower cooling rates in the upper layers which led to a longer transformation time for the austenite.

General investigations on anisotropic mechanical properties of thin walled WAAM-structures were conducted by Sun et al. [15]. They determined inferior mechanical properties
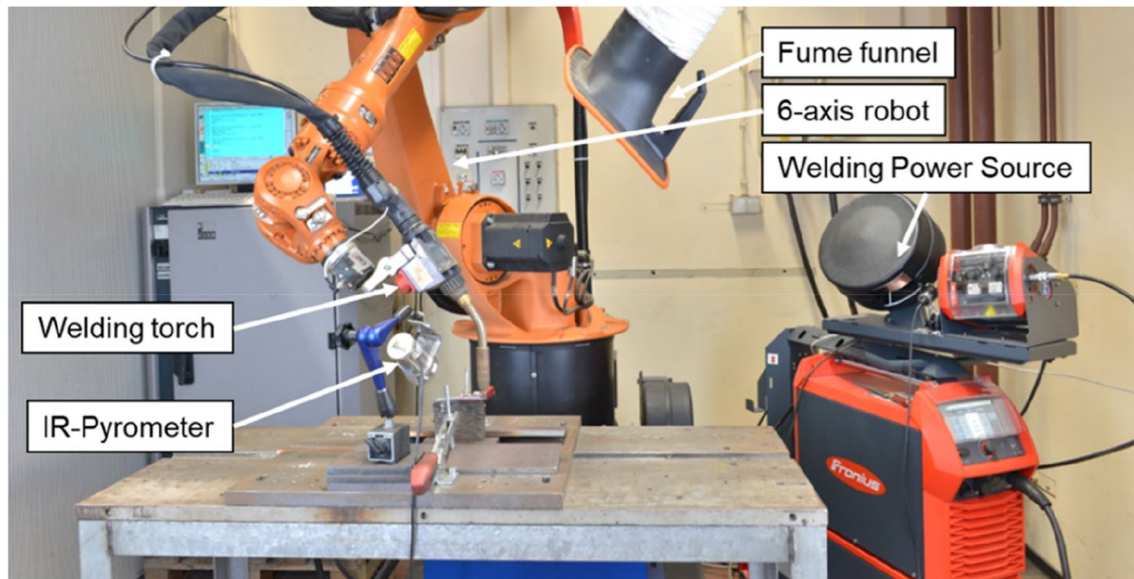
Fig. 1 Welding setup

for specimens longitudinal to the building direction. Direct image correlation measurements showed a strain concentration at the interlayer areas resulting from interlayer softening by inhomogeneous microstructure, nonuniform strength distribution, and various textures.

Studies on the application of active cooling during wire arc additive manufacturing can be found in [16, 17]. However, in these studies, aluminum alloys were investigated. The cooling concept investigated here was "near immersion active cooling" (NIAC), where the substrate was placed in a tank filled with water. The water rose while the structure was build up. That led to a reduction of heat accumulation which resulted in smaller differences of the mechanical properties longitudinal und transversal to the building direction. The yield and tensile strength showed to be not affected by active cooling. Reisgen et al. [18] evaluated different cooling strategies using steel (G3Si1). Active cooling via water bath,

high-pressure air, and aerosol were compared regarding the resulting cooling times, microstructure, and hardness. The best cooling effect was achieved by the water bath cooling, followed by the air cooling. The aerosol cooling showed the smallest effect. However, the water bath cooling generally constrains the degrees of freedom when fabricating complex parts. Accordingly, high-pressure air cooling is considered as the most promising cooling method. Henckell et al. [19] investigated the influence of different cooling gases and cooling positions on the heat accumulation during a continuous WAAM process for generation of a tube. The best cooling effect was achieved by the usage of nitrogen with 5% hydrogen as cooling gas. Generally, the effects of active cooling on the thermal cycles for the wire arc additive manufacturing of steel were investigated, but studies on the mechanical properties of high strength steel WAAM parts with different temperature profiles resulting from active cooling are not available yet.

Fig. 2 Build-up strategy for thin walled structures
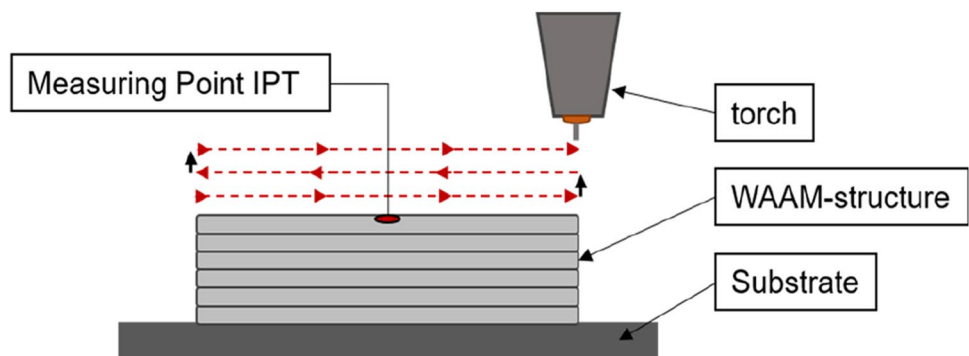
Table 1 Chemical analysis of the used filler wire

	C	Si	Mn	P	S	Cr	Mo	Ni
3dprint AM80	0.107	0.359	1.69	0.0111	0.0033	0.384	0.594	2.18
	Al	Co	Cu	Nb	Ti	V	W	
3dprint AM80	0.0092	0.0063	0.0551	0.0021	0.0015	0.0079	0.006	

**Table 2** Manufacturing parameters for the investigated specimens

| Specimen	v_{wire} in m/min	v_{weld} in cm/min	IPT in °C	Cooling	I in A	U in V	E in kJ/cm
W-2.7–200	2	25	200	Passive	82±1.9	13.8±0.2	2.7
W-4.6–200	6	45	200	Passive	198.3±3.6	18±0.1	4.8
W-2.7–400	2	25	400	Passive	81.4±1.0	13.8±0.3	2.7
W-4.6–400	6	45	400	Passive	188.8±4.2	18±0.2	4.5
C-2.7–200	2	25	200	Compressed air	83.3±1.,7	13.8±0.3	2.8
C-4.6–200	6	45	200	Compressed air	192.8±4.1	18±0.3	4.6
C-2.7–400	2	25	400	Compressed air	83.1±0.7	13.9±0.1	2.8
C-4.6–400	6	45	400	Compressed air	190.7±4.6	18.1±0.1	4.6

3 Experimental work

The welding setup to fabricate the thin walled samples is shown in Fig. 1. It consists of a welding power source (Fronius TPS500i) which is linked to a robotic handling system (KUKA 16–2) where the torch is mounted. That allows repeatable conditions for the manufacturing of the wall structures. The welding parameters were monitored by a welding process data scanner (HKS Weldscanner) which logs the current, the voltage, and the wire feed. An infrared pyrometer (optris CTlaser3MH2) was used to measure the interpass temperature. The measuring point was, as depicted in Fig. 2, in the middle of the wall on the top layer. To gain more information about the thermal cycle, all manufacturing processes of the walls were captured by thermography.

In order to investigate the influence of thermal cycles on the mechanical properties of the welded structures, a thin walled structure with a length of 350 mm and a height of 160 mm was fabricated. The build-up strategy for those walls is depicted in Fig. 2. First step is the deposition of a single weld bead on the substrate plate. The interpass temperature was measured by IR-pyrometry ($\varepsilon = 0.89$) in the middle of the last welded layer. As soon as the desired, preliminary defined interpass temperature is reached, the next bead is welded on the previously welded bead, as compared in Fig. 2. This process repeats
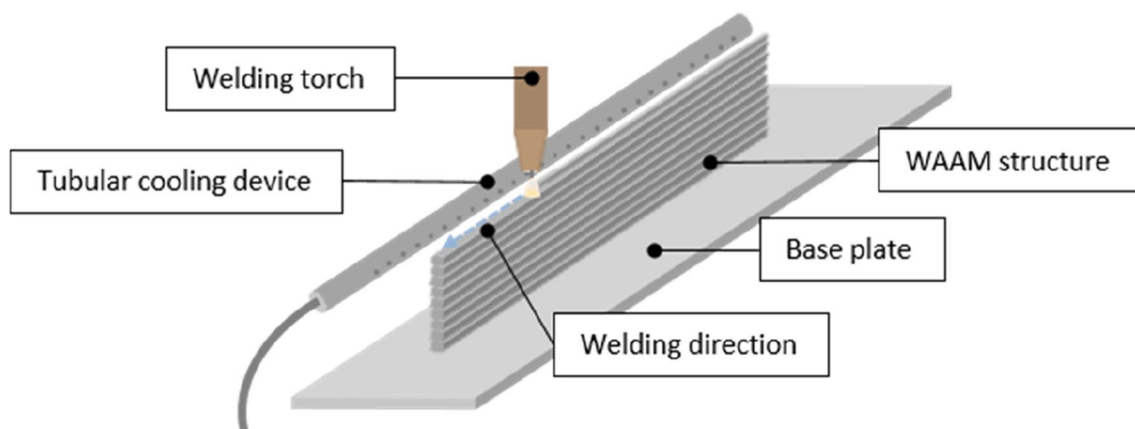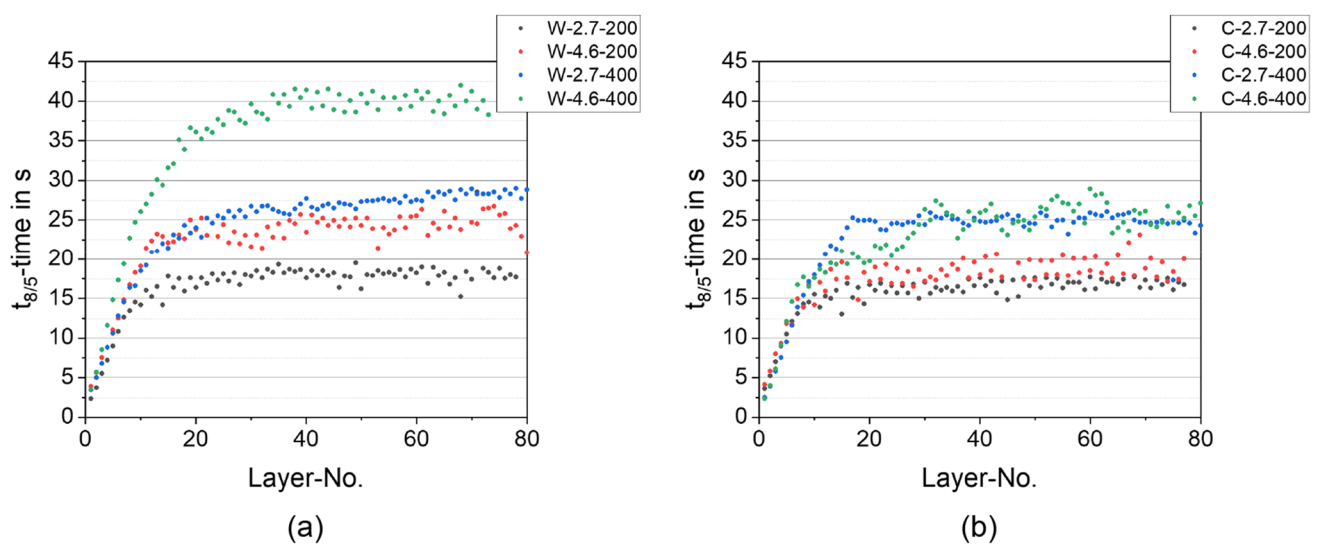

Fig. 3 Applied method for active cooling of the thin walled structures
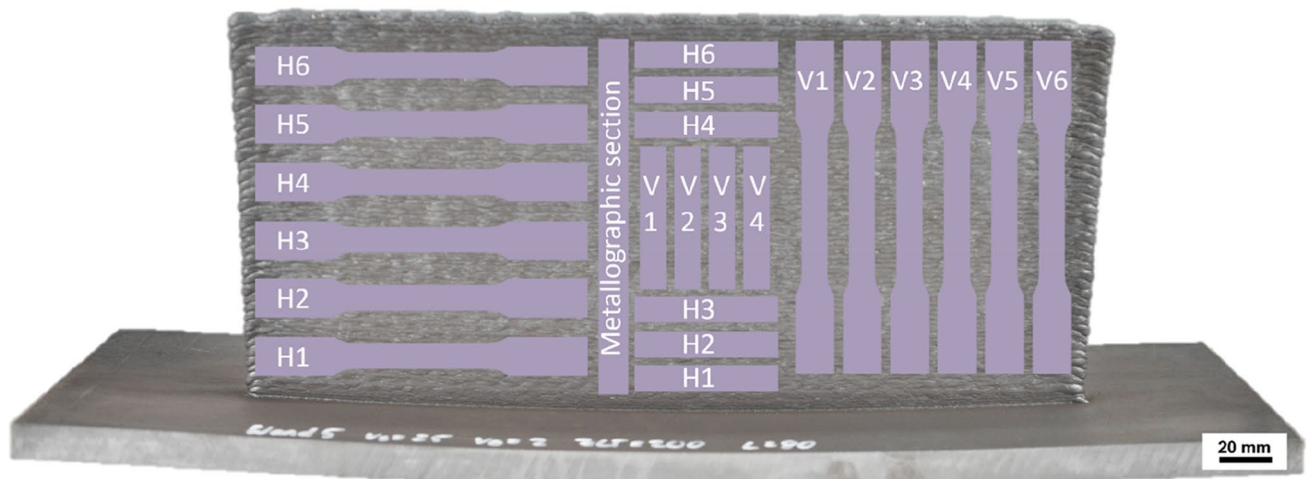
Fig. 4 Extraction positions of the specimens (tensile test specimens, Charpy-V specimens, and metallographic section) from the WAAM structure
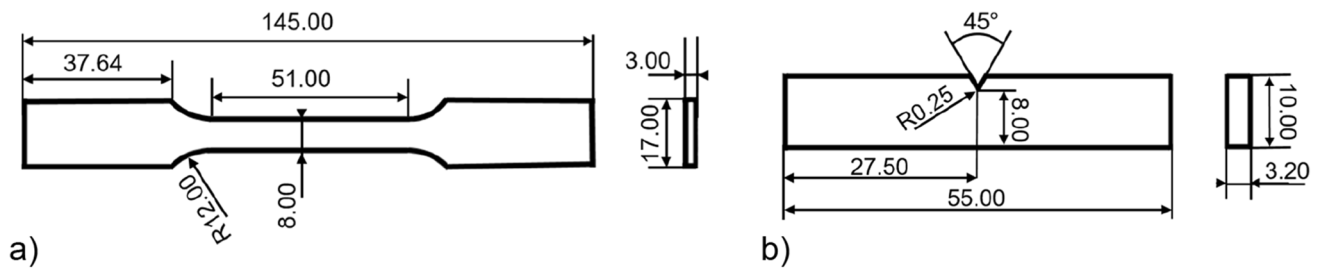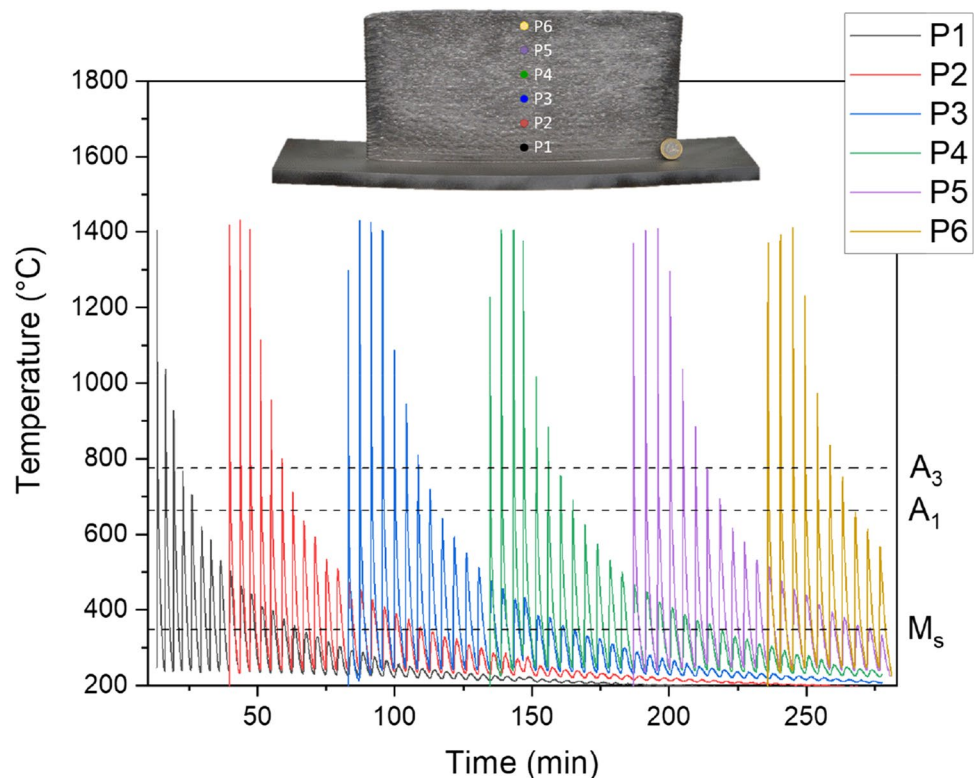

Fig. 5 Geometry of **a** the tensile test specimens and **b** the Charpy-V specimens

Fig. 6 $t_{8/5}$-times of each layer for **a** passive cooling and **b** active cooling

Fig. 7 Time–temperature development of 6 points along the build-up direction (illustrative for W-2.7–200)

until a desired height or number of layers is reached. The welding direction changes after each layer since accumulation of material at the welding start point shall be avoided.

As build-up material, a solid wire with a diameter of 1.2 mm named 3dprint AM80 was used, which is a high strength steel with a yield strength of ~ 820 MPa and a tensile strength of ~ 920 MPa. The chemical composition is given in Table 1. The shielding gas was M21 (82% Argon, 18% CO_2) with a flow rate of 16 l/min. As substrate a S355J2 + N sheet metal with a thickness of 15 mm was used, here, the dilution from the base plate was not considered since the extracted specimens are at least 10 mm (5 weld beads) away from the base plate.

As the aim of this study is to investigate the influence of thermal cycles on the mechanical properties of high strength steel, wall structures were manufactured under variation of energy input, interpass temperature, and cooling. The test plan is given in Table 2.

The active cooling was implemented by compressed air which flowed through a perforated tube in order to create a linear inflow. The flow rate at the wall surface was measured by an impeller anemometer and had a constant rate of 12 m/s. Air cooling was used for this work because it is readily available in fabrication shops, is inexpensive, and easily transported to the part. The tube was moved manually with increasing height of the wall to keep the inflow at the top layers of the specimen (Fig. 3).
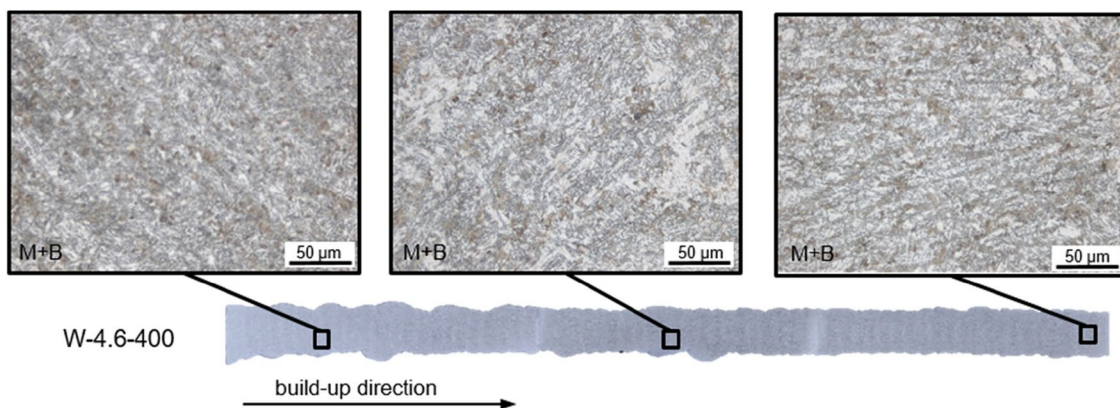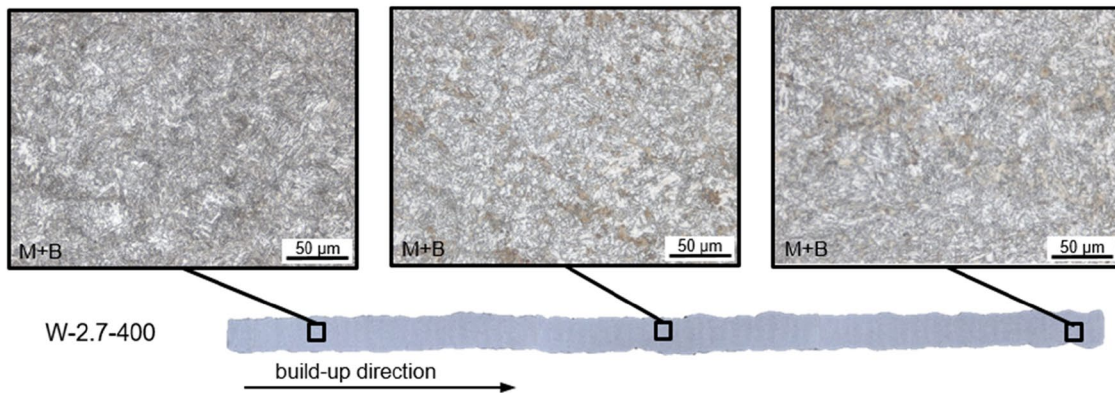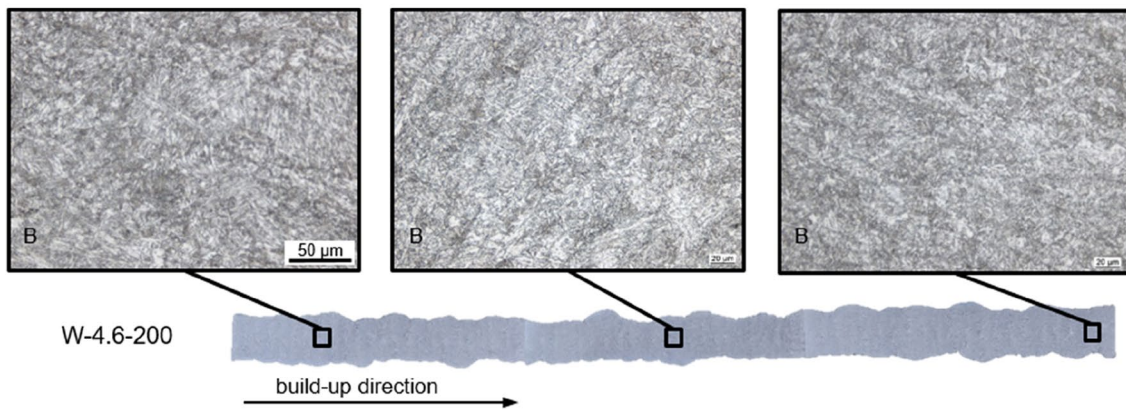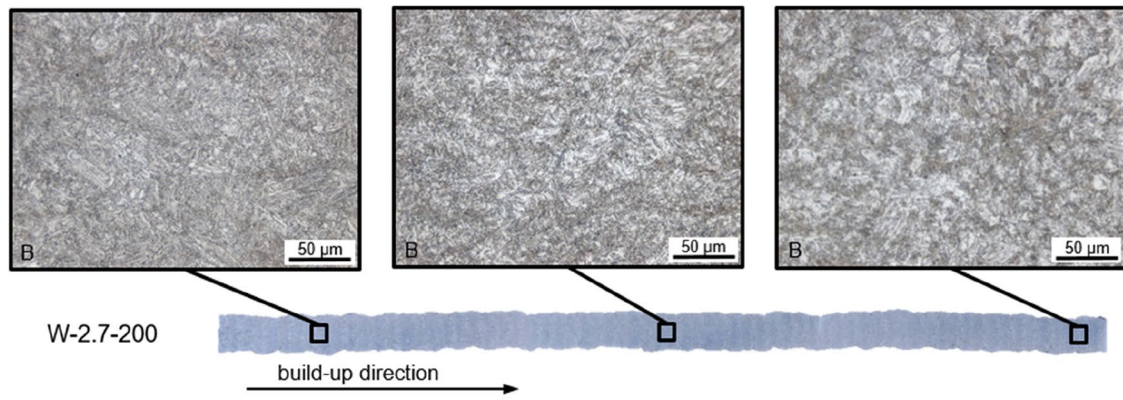
3.1 Specimen preparation

In order to characterize the mechanical properties as well as the microstructure, the following specimens were extracted from the WAAM walls. As one can see in Fig. 4, six tensile test specimens were extracted horizontally and six more were extracted vertically to the build-up direction. In the middle of the wall, Charpy-V specimens were extracted — six horizontally and four vertically to the building direction. Additionally, one long rectangular specimen was extracted for metallography and hardness measurements.
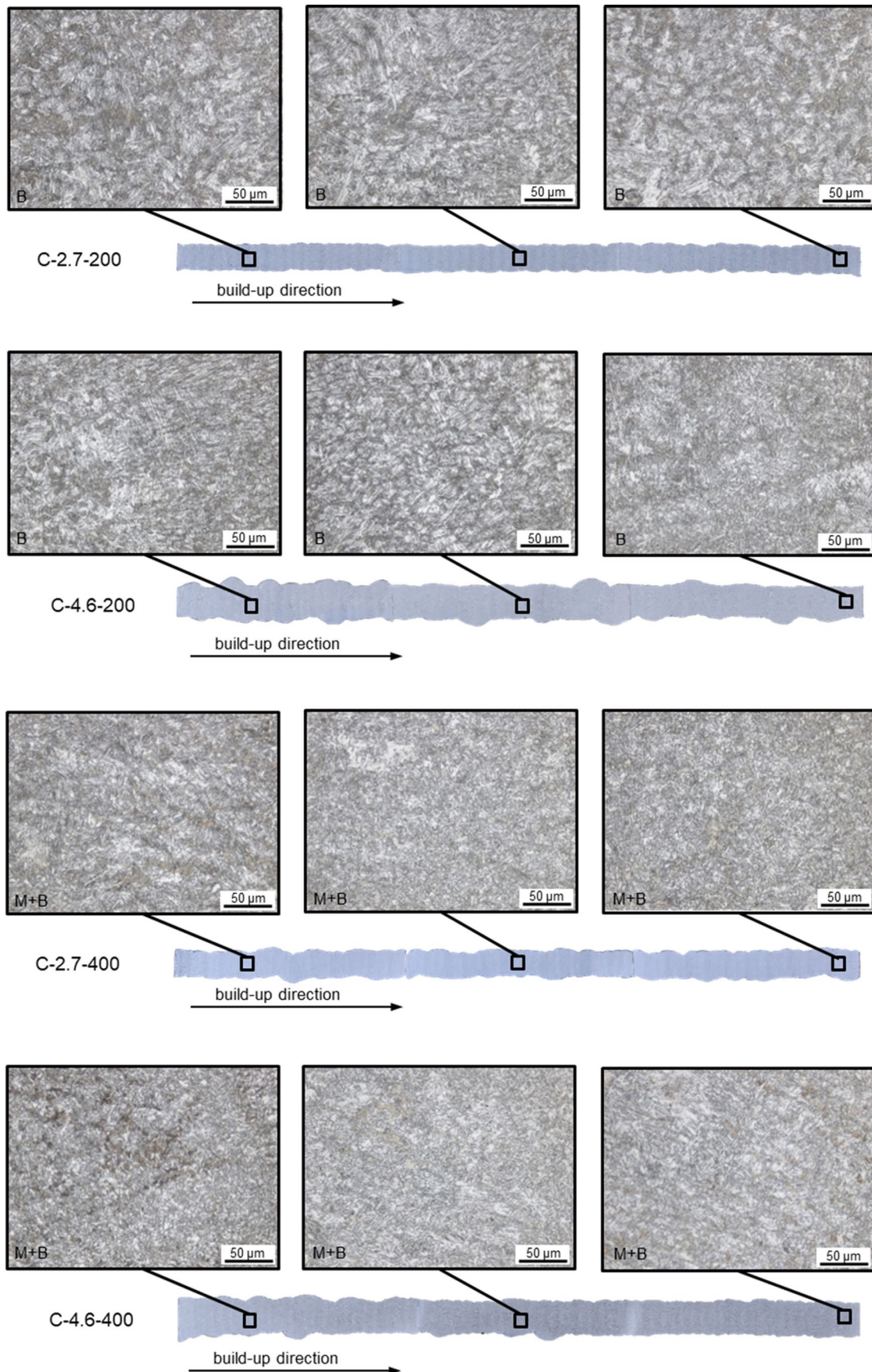
3.2 Hardness measurements and microstructure

The long rectangular specimens were prepared metallographically, etched with Nital, and micrographs were taken on three different positions: close to the base plate, in the middle of the wall, and at the last welded layers. After that, Vickers hardness measurements were conducted using a ZwickRoell ZHU250CL hardness testing machine. For the indentions, a force of 10 kg with an indention time of 15 s was used. The indentions were set in a line in the middle of the sample along the build-up direction with a distance of 2 mm.

Fig. 8 Microsections of the specimens with passive cooling. *M* martensite, *B* bainite ▶

W-2.7-200

build-up direction

W-4.6-200

build-up direction

W-2.7-400

build-up direction

W-4.6-400

build-up direction

C-2.7-200
build-up direction

C-4.6-200
build-up direction

C-2.7-400
build-up direction

C-4.6-400
build-up direction

◄**Fig. 9** Microsections of the specimens with active cooling: *M* martensite, *B* bainite

3.3 Mechanical testing

The geometry of the tensile test specimens was designed according to DIN 50,125 [20]. For better accessibility of the strain gauges, the length Lc was expanded to 51 mm. The measuring length Lo for the proportional elongation at fracture remained 30 mm to keep the comparability. All geometric dimensions of the tensile test specimens can be found in Fig. 5.

The geometry for the Charpy-V specimens was chosen on behalf of DIN EN ISO 148–1 [21] with a length of 55 mm and a width of 10 mm. Due to the width of the thin walled samples, the thickness of the specimens needed to be modified. For all specimens, a thickness of 3.2 mm was chosen. In order to compare the toughness in different sections of the wall, all specimens were tested at a constant temperature of −40 °C. The radius of the hammer fin was 2 mm with 300 J.

## 4 Results and discussion

4.1 Thermal cycle and $t_{8/5}$-times

The $t_{8/5}$-times for each layer calculated from the pyrometer measurements are displayed in Fig. 6. For the parameter set with low heat input and low interpass temperature

(W-2.7–200), the $t_{8/5}$-times were with 17 s the lowest. When the energy input increased, the $t_{8/5}$-times stabilized around 25 s. Comparable $t_{8/5}$-times are achieved with low heat input but high interpass temperature ($t_{8/5}$-time ≈ 29 s). The highest $t_{8/5}$-time with 40 s resulted from high interpass temperatures and high energy inputs.

By the application of active cooling, the $t_{8/5}$-times were reduced especially for the specimens with high energy input. For the specimen with 4.6 kJ/cm energy input and an interpass temperature of 400 °C, the cooling time could be reduced from 40 to 26 s. Also for the specimen with high energy input and low interpass temperature, the $t_{8/5}$-time decreased from ≈ 25 to ≈ 20 s, whereas the cooling times for specimens with low energy input were reduced less (29 s to 25 for 400 °C interpass temperature or 18 to 17 s for 200 °C interpass temperature).

Due to the layerwise build-up strategy, the deposited layers are frequently reheated to temperatures greater than A_1 or A_3 where austenitization takes place. So it can be concluded that not only the $t_{8/5}$-time for the first solidification is a measure for the resulting microstructure and the mechanical properties but also parameters like peak temperatures, holding times, number of reheating, and minimal temperatures as interaction of each other.

Figure 7 shows exemplary the time–temperature development at six single points in the middle of the wall. It can be seen that for example, P6 has long holding time above A_1 and a short holding time in the temperature interval between A_1
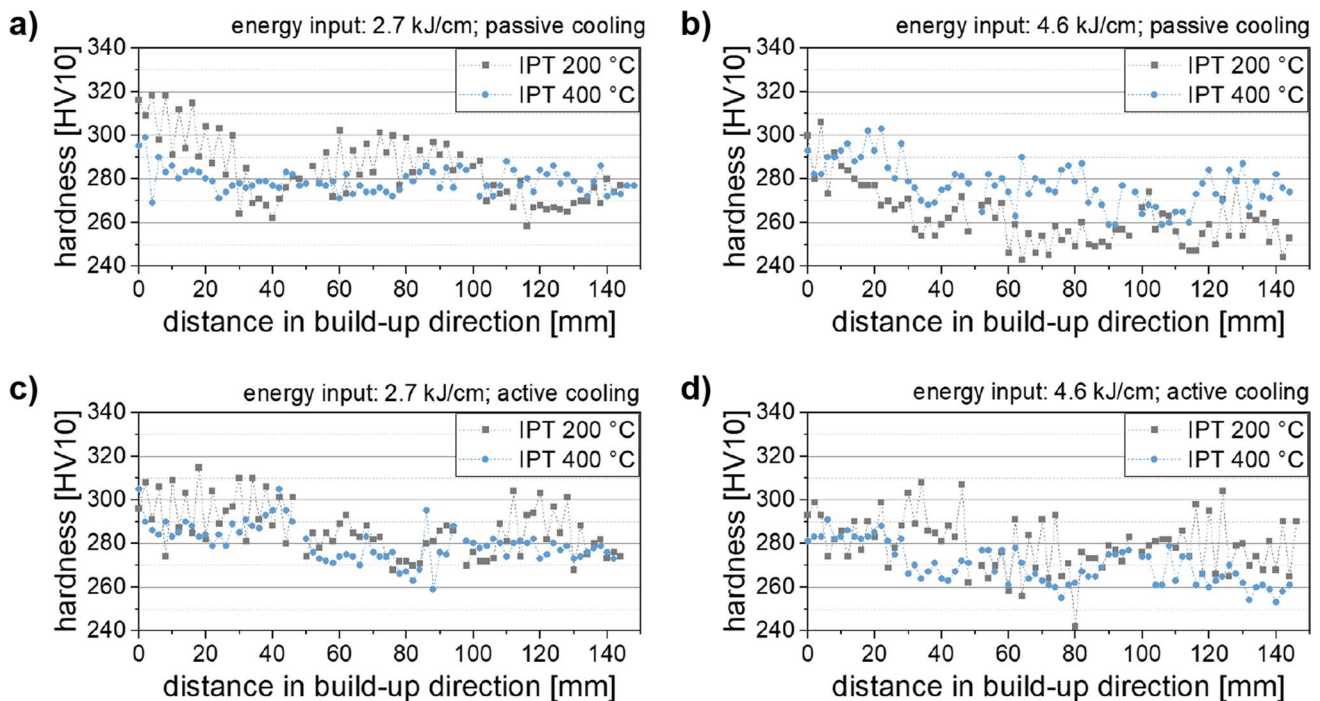
Fig. 10 Hardness distribution along build-up direction for **a** W-2.7–200 & W-2.7–400; **b** W-4.6–200 & W-2.7–400; **c** C-2.7–200 & C-2.7–400; **d** C-4.6–200 & C-4.6–400

Fig. 11 Boxplot of the hardness measurements of all specimens, pc = passive cooling, ac = active cooling
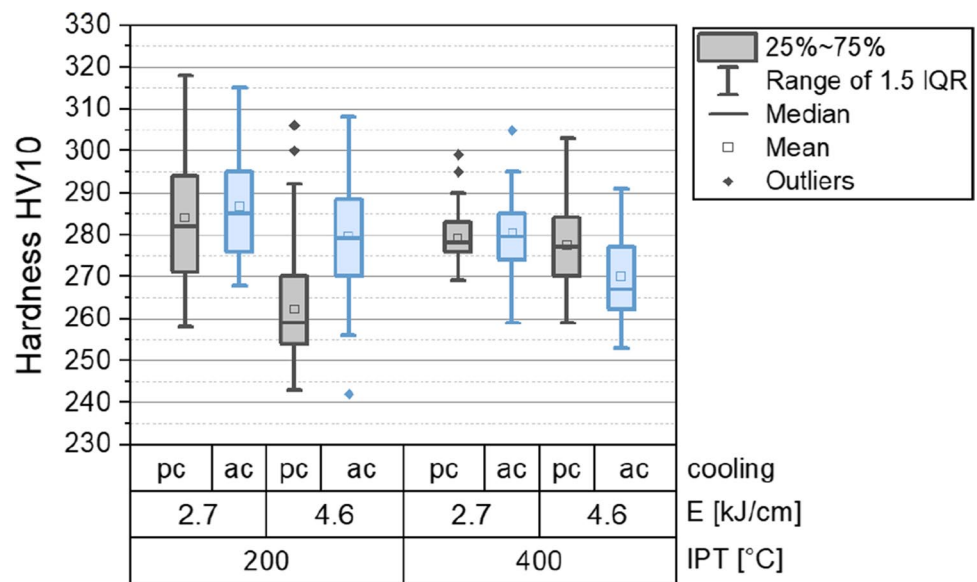
and M_s (martensite start temperature) which is basically the temperature range where the ferrite and the cementite forms the microstructure resulting in martensite, bainite, pearlite, or ferrite, depending on the cooling/holding time.

As a result of that, the top or bottom layers may have another microstructure and hence the mechanical properties along the building direction may vary.

4.2 Microstructure and hardness

To analyze the differences between top and bottom layers, magnifications of the microstructure were taken and displayed in Fig. 8 and Fig. 9. In general, the microstructure was very fine-grained. It was judged to consist mainly of upper and lower bainite, since the acicular structure is typical for bainite and hardness is around 240 and 340 HV1. Moreover, the CCT diagram shows the formation of bainite in a wide range of cooling rates. In some cases

(e.g., W-2.7–400, W-4.6–400, C-2.7–400, and C-4.6–400), a phase with hardness of around 600 HV 0.01 was detected and judged to be martensite. The martensite either transformed successively through comparatively fast cooling, or from retained austenite, depending on the interpass temperature and the energy input. However, in most cases, the percentage of martensite was low (smaller than 10%) and the area fractions were small (< 20 μm).

The hardness measurements showed generally a large scatter; but nevertheless, it can be seen that the hardness along the build-up direction decreased. In the case of high energy input the hardness of the specimen with an interpass temperature of 400 °C (W-4.6–400) exhibited higher hardness values than those samples with lower interpass temperature (W-4.6–200). (Fig. 10b).

Figure 11 provides an overview of the effects of the varied parameter on the hardness. In the case of low interpass temperatures, the hardness increased when applying active
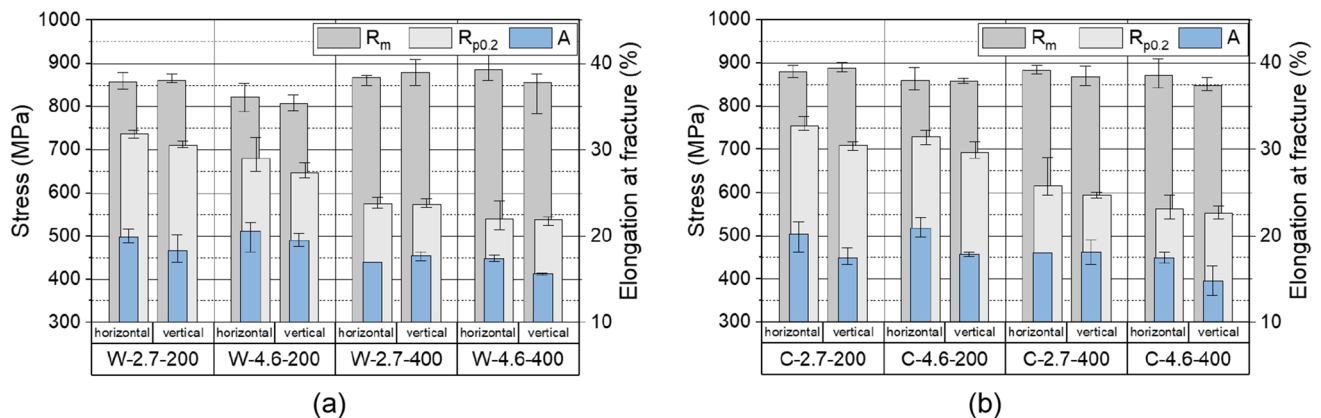
Fig. 12 Mechanical properties of the specimens with **a** passive cooling and **b** active cooling (*n* = 6, except for elongation at fracture)
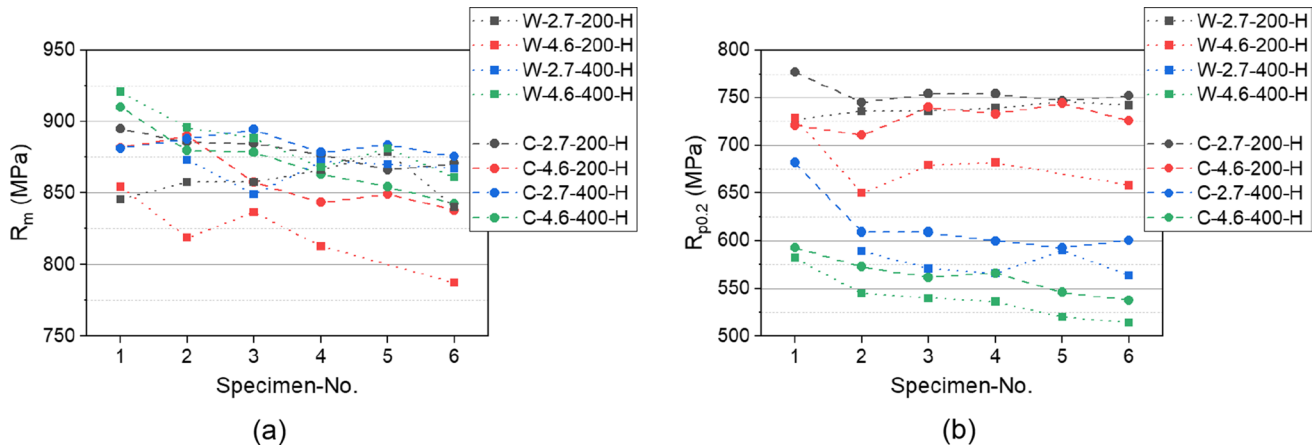
Fig. 13 The development of the **a** tensile strength and **b** the yield strength (distance to the base plate increased from specimen 1 to specimen 6)

cooling (e.g., W-4.6–200 and C-4.6–200). This may be an effect of the formation of lower bainite due to higher cooling rates. In the case of higher interpass temperatures, the increase of hardness (W-4.6–400 compared to W-4.6–200) can be explained by the presence of martensite. The austenite formed to upper bainite and martensite after final cooling. By applying active cooling, the austenite transformed to bainite at an earlier stage which resulted in lower amounts of martensite and hence in lower hardness values (compare W-4.6–400 and C-4.6–400). This was confirmed by the microsections in Fig. 8 and Fig. 9 as well, where the amount of martensite appeared lower in the specimen with active cooling compared to the specimen with passive cooling.

Generally the scatters, more specifically the min to max span and the percentiles, were larger in the case of interpass temperatures of 200 °C which could be caused by the hardness gradient in build-up direction.

4.3 Mechanical properties

The mechanical properties were determined by the execution of tensile tests. The results are displayed in Fig. 12. The tensile strength of all specimens varied between 780 and 940 MPa. The yield strength showed a strong sensitivity to the manufacturing parameters and ranged from 500 to 780 MPa. The lowest elongation at fracture was 13.1% for C-4.6–400 vertical specimen and 22.7% for the W-4.6–200-horizontal specimen. Concerning the load direction (horizontal/vertical), it can be observed that in almost every case, the specimens vertical to the build-up direction showed inferior properties regarding tensile strength, yield strength, and elongation at fracture. Findings from Sun et al. [15] can be confirmed also for this material. Sun stated that the inferior mechanical properties longitudinal to the build-up direction result from interlayer softening due to
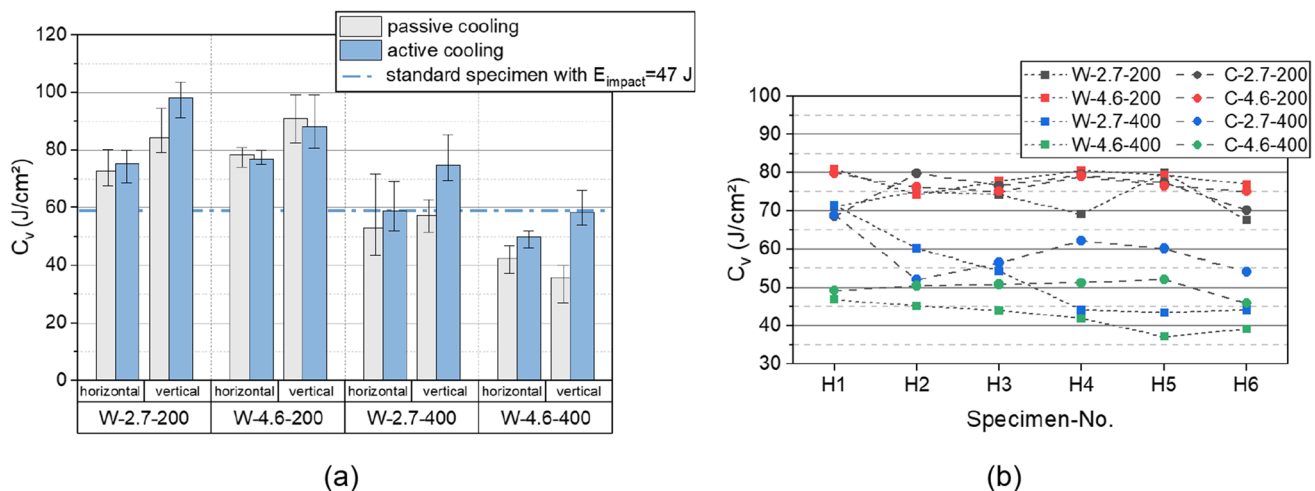
Fig. 14 Charpy impact energy per cm² **a** as comparison of all specimens **b** with increasing distance to the base plate (H1 is close to the base plate and H6 close to the top layers)

inhomogeneous microstructure, nonuniform strength distribution causing strain and stress concentration. In addition to Sun´s study, this work shows the presence of inferior properties longitudinal to the build-up direction regardless of the energy input, interpass temperature, or cooling strategy.

Furthermore, it can be seen in Fig. 12 a that the tensile strength increased with higher interpass temperature while the yield strength and the elongation at fracture decreased. When welding at low interpass temperatures with higher energy input, both, the tensile strength and the yield strength, decreased. This can be referred to longer holding times in the temperature range where bainite was formed. For high energy input, more upper bainite was formed, which has slightly inferior mechanical properties than lower bainite [22]. The formation of upper bainite could be counteracted by the application of an active cooling, which lowered the holding time in the bainitization temperature range and thus the formation of lower bainite was supported. This effect could be observed by comparing W-4.6–200 and C-4.6–200. Here, the tensile strength increased from 820 to 860 MPa (horizontal) and the yield strength increased from 680 to 730 MPa.

The reduction of the yield strength, as a result of high interpass temperatures, conversely cannot be completely avoided by active cooling.

Regarding the development of the mechanical properties along the build-up direction, Fig. 13 shows that with increasing distance to the base plate the tensile strength as well as the yield strength decreased. For the tensile strength (Fig. 13a), this effect was distinct for specimens with high energy input. It confirms the finding that long holding times in the bainitization temperature range promote the formation of upper bainite resulting in inferior strengths. Considering Fig. 7, the holding time between A_1 and M_s enlarged with increasing distance to the base plate.

4.4 Charpy impact test results

The Charpy impact tests were conducted in accordance to DIN EN ISO 148–1 [23] and the results are depicted in Fig. 14. It must be taken into account that the depicted energy is the energy per cm^2 because the used specimens were thinner than the standard Charpy-V specimens. To compare the impact energy tested at -40 °C with standard Charpy-V specimen, the target energy of 47 J can be set in relation to the cross section, which would be 58.75 J/cm^2.

The specimens with an interpass temperature of 200 °C showed higher absorbed impact energies than those with high interpass temperatures. A possible reason might be the presence of more brittle martensite in the high interpass temperature specimens. With increasing energy input at low interpass temperatures (W-2.7–200 and W-4.6–200), the impact energy increased, which substantiates the

assumption that more upper bainite formed as consequence of the extended holding times in the bainitization temperature range. That was not the case for energy increase at high interpass temperatures since the microstructure was reheated more frequently to temperatures above A_1 and A_3. Consequently, parts of the microstructure re-transformed to austenite which kept untransformed until the final cooling of the WAAM structure.

The application of active cooling increased the absorbed impact energy for all specimens, except those made from W-4.6–200. That can be explained by the suppression of retained austenite and hence the formation of martensite since the single layers were exposed to temperatures $> A_1$ and A_3 less frequently and for a shorter period of time. For the specimen W-4.6–200 e.g. C-4.6–200, this effect could not be observed because there was no martensite detected in the microstructure. The active cooling led to more upper bainite and less lower bainite. Figure 14 b depicts the impact energy for specimens with increasing distance to the base plate. Especially for the specimens with high interpass temperature with passive cooling, a decrease of the impact energy can be identified.

5 Summary

The aim of this study was to determine the effects of different thermal cycles on the microstructure and the mechanical properties of thin walled high-strength steel structures. The specimens were fabricated with interpass temperatures of 200 °C and 400 °C and energy inputs of 2.7 kJ/cm and 4.6 kJ/cm. Additionally, one set of specimens was fabricated with the same parameters applying active cooling. By the conduction of tensile tests, Charpy-V tests and the analysis of the hardness and microstructure, the following conclusions could be drawn:

- High interpass temperature led to formation of martensite during final cooling resulting in high R_m, low $R_{p0.2}$, and low C_v.
- High energy input at low interpass temperature led to formation of upper bainite which lowered R_m and $R_{p0.2}$, and increased C_v.
- High energy input at high interpass temperature supported the formation of martensite and thus lowered the Charpy impact energy.
- The effect of active cooling led to a strong increase of R_m and $R_{p0.2}$ in the case of low interpass temperatures, since active cooling at low interpass temperatures supports formation of lower bainite instead of upper bainite.
- In the case of high interpass temperature, the above-mentioned effect of active cooling was less distinct.

Further research will address the evolution of the microstructure during frequent reheating. The findings obtained shall be extended to the fabrication of voluminous elements or the fabrication of complex parts. Additionally, a suitable heat treatment shall be identified to dissolve the martensite which led to unfavorable mechanical properties.

Declarations

Conflict of interest The authors declare s no competing interests.

References

1. Adriaenssens S, Block P, Veenendaal D, Williams CJK (eds) (2014) Shell structures for architecture: form finding and optimization. Routledge, London
2. Feldmann M, Kühne R, Citarelli S, Reisgen U, Sharma R, Oster L (2019) 3D-Drucken im Stahlbau mit dem automatisierten wire arc additive manufacturing. Stahlbau 88(3):203–213
3. Feucht T, Lange J, Erven M (2019) 3-D-Printing with steel: additive manufacturing of connection elements and beam reinforcements. ce/papers, 3, (3–4), 343–348
4. Reimann J, Henckell P, Ali Y et al (2021) Production of topology-optimised structural nodes using arc-based, additive manufacturing with GMAW welding process. J Civ Eng Constr 10(2):101–107
5. Suryakumar S, Karunakaran KP, Chandrasekhar U, Somashekara MA (2013) A study of the mechanical properties of objects built through weld-deposition. Proceedings of the Institution of Mechanical Engineers, Part B: Journal of Engineering Manufacture 227(8):1138–1147
6. Rafieazad M, Ghaffari M, Vahedi Nemani A, Nasiri A (2019) Microstructural evolution and mechanical properties of a low-carbon low-alloy steel produced by wire arc additive manufacturing. Int J Adv Manuf Technol 105(5–6):2121–2134
7. Sun L, Jiang F, Huang R, Yuan D, Guo C, Wang J (2020) Microstructure and mechanical properties of low-carbon high-strength steel fabricated by wire and arc additive manufacturing. Metals 10(2):216
8. Soliman, M.A.: 'Phase transformations and mechanical properties of new austenite-stabilised bainite steels' (Pieper, Clausthal-Zellerfeld, 2008, 1st edn.)
9. Dai Y, Yu S, Huang A, Shi Y (2020) Microstructure and mechanical properties of high-strength low alloy steel by wire and arc additive manufacturing. Int J Miner Metall Mater 27(7):933–942
10. Yildiz AS, Davut K, Koc B, Yilmaz O (2020) Wire arc additive manufacturing of high-strength low alloy steels: study of process parameters and their influence on the bead geometry and mechanical characteristics. Int J Adv Manuf Technol
11. Dirisu P, Ganguly S, Mehmanparast A, Martina F, Williams S (2019) Analysis of fracture toughness properties of wire + arc additive manufactured high strength low alloy structural steel components. Materials Science and Engineering: A 765:138285
12. Rodrigues TA, Duarte V, Avila JA, Santos TG, Miranda RM, Oliveira JP (2019) Wire and arc additive manufacturing of HSLA steel: effect of thermal cycles on microstructure and mechanical properties. Addit Manuf 27:440–450
13. Duarte VR, Rodrigues TA, Schell N, Santos TG, Oliveira JP, Miranda RM (2021) 'Wire and arc additive manufacturing of high-strength low-alloy steel: microstructure and mechanical properties. Adv Eng Mater 2001036
14. Bourlet C, Zimmer-Chevret S, Pesci R, Bigot R, Robineau A, Scandella F (2020) Microstructure and mechanical properties of high strength steel deposits obtained by wire-arc additive manufacturing. Journal of Materials Processing Technology, 116759
15. Sun L, Jiang F, Huang R, Yuan D, Guo C, Wang J (2020) Anisotropic mechanical properties and deformation behavior of low-carbon high-strength steel component fabricated by wire and arc additive manufacturing. Materials Science and Engineering: A, 787, 139514
16. Da Silva LJ, Souza DM, de Araújo DB, Reis RP, Scotti A (2020) Concept and validation of an active cooling technique to mitigate heat accumulation in WAAM. Int J Adv Manuf Technol 107(5–6):2513–2523
17. Scotti FM, Teixeira FR, Silva LJD, De Araújo DB, Reis RP, Scotti A (2020) Thermal management in WAAM through the CMT Advanced process and an active cooling technique. Journal of Manufacturing Processes 57:23–35
18. Reisgen U, Sharma R, Mann S, Oster L (2020) Increasing the manufacturing efficiency of WAAM by advanced cooling strategies. Weld World 64(8):1409–1416
19. Henckell P, Günther K, Ali Y, Bergmann JP, Scholz J, Forêt P (2017) The influence of gas cooling in context of wire arc additive manufacturing—a novel strategy of affecting grain structure and size', in TMS, T.M.M.&.M.S. (Ed.): 'TMS 2017 146th Annual Meeting & Exhibition Supplemental Proceedings' (Springer International Publishing, Cham), 147–156
20. DIN 50125: Prüfung metallischer Werkstoffe – Zugproben, Dezember 2016
21. DIN EN ISO 148–1: Metallsiche Werkstoffe - Kerbschlagbiegeversuch nach Charpy, Mai 2017
22. Schade C, Murphy T, Lawley A, Doherty R. Microstructure and mechanical Properties of a Bainitic PM Steel
23. DIN EN ISO 148–1: 'Kerbschlagbiegeversuch nach Charpy', Mai 2017

Publisher's note Springer Nature remains neutral with regard to jurisdictional claims in published maps and institutional affiliations.